Computing and Visualization in Science manuscript No.
(will be inserted by the editor)

Visualising Deformation Fields Computed by Non-Linear Image Registration

Marc Tittgemeyer, Gert Wollny, Frithjof Kruggel

Max-Planck-Institute of Cognitive Neuroscience, Stephanstr. 1a, D-04103 Leipzig, Germany
e-mail: {tittge,wollny,kruggel}cns.mpg.de

The date of receipt and acceptance will be inserted by the editor

Abstract. Magnetic resonance imaging (MRI) is used in clinical routine to map the brain's morphology. Structural changes due to brain growth, ageing, surgical intervention or pathological processes may be detected by non-linear image registration of time-series imaging data. The resulting displacement field is large and therefore, hard to interpret. For a simplified but sufficient description of the displacement field contraction mapping is proposed to detect vector field singularities. This allows the detection and analysis of singularities of any order as critical points which reflect the topology of the vector field. An application demonstrates how this method helps to increase the understanding of pathological processes in the brain.

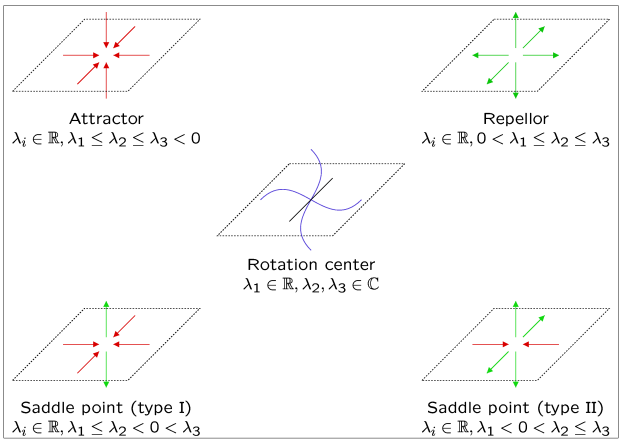

Fig. 1. Classification criteria for critical points (after Abraham and Shaw [1]). λ_i denote the eigenvalues of the phase portrait to a critical point.

1 Introduction

High-dimensional vector fields are a result of observed measurements or simulated processes in a variety of application domains (e.g., geophysics, meteorology, or medicine). In order to improve the understanding of underlying dynamics it is useful to characterize the vector field by its critical points. The most prominent critical points are attractors, repellors and vortices (rotation centers). A concise classification scheme for critical points (Fig. 1) by their so-called phase portrait has been introduced by Abraham and Shaw [1]. Critical points characterize the high-dimensional vector field as a sparse set of features, that are sufficient to understand the bahaviour of the simulated physical process and its topology.

However, the detection and visualization of critical points is still an active research area where rather sophisticated mathematical methods have been employed [12]. Established are topological methods as introduced by Helman and Hesselink [13] that decompose vector fields in different global regions of interest based on local linear approximations of the Jacobian. Higher-order approximations yield different decompositions [22]. Philippou and Strickland [19] introduced a geometrical method where critical points are found at the intersection of lines tangent with the vector orientation (or at the intersection of planes orthogonal to the vectors). Other widely employed methods are based on the Poincaré-Hopf index theorem [e.g., 10].

In our application, changes of brain structure due to brain growth, ageing, surgical intervention or pathological processes are monitored by time-series examinations using magnetic resonance imaging (MRI). MR images are given as 3D matrices of intensity values. Beyond usual comparison of the image data, which is still the gold standard in clinical neuro science, structural changes with time my be detected by non-linear registration of the imaged brain. The result of the registration algorithm is a vector field which maps one image onto another. This displacement field reflects the structural change that acted on the brain.

Due to the finite spatial resolution of the images, the displacement field is given on a discrete grid. Since, for example, growth or atrophying processes take place in finite sub-compartments of the brain, representing critical points by point sources is an over-simplification. Most conventional methods fail therefore to detect critical points within medical vector fields. Thus, in our application critical points are not regarded as infinitesimally small.

We rather propose a novel method that is based on the contraction mapping theorem [15]. For an application to a patient suffering from a head contusion (trauma) we will illustrate how non-rigid registration and critical points analysis may help to understand the disease process.

2 Non-rigid image registration

Image registration is usually achieved by applying a vector field transformation to one image in order to match another (reference) image with respect to a given cost function describing the image differences. In practice, these transformations must accommodate both very complex and large deformations. The mathematical framework to carry out such task with respect to the discipline of computational anatomy has been compiled by Grenander and Miller [11].

Image matching of deformable structures has received considerable attention during the last decade [16]. The high dimensional transformations involved in deformable registration generally make the problem ill-conditioned (i.e., many possible solutions exists), so that additional constraints are needed to obtain a physically plausible result [2, 3, 9, 17]. Recently, Musse et al. [18] or Christensen [8] address also the topological issues involved with small- and large-distance, non-linear transformations.

Bio-mechanically plausible transformations are constrained to be consistent with the physical properties of deformable elastic solids. To understand how elastic image matching works, consider the deforming image to be embedded in a 3D elastic medium. The medium is subjected to distributed internal forces, which reconfigure it, and lead the image to match a target. In linear elastic media, the displacement vector field $\mathbf{u}(\mathbf{x})$ resulting form internal driving forces $\mathbf{F}(\mathbf{x})$ (called *body forces*) obeys the Navier-Stokes equilibrium equations for linear elasticity:

$$\mu\nabla^2\mathbf{u} + (\lambda+\mu)\boldsymbol{\nabla}(\boldsymbol{\nabla}\cdot\mathbf{u}) = \mathbf{F}(\mathbf{u}), \quad \forall\,\mathbf{x}\in\mathbb{R}^n. \tag{1}$$

Here $\mathbb{R}^n$ is the discrete lattice representation of the image, $\boldsymbol{\nabla}\cdot\mathbf{u} = \partial u_j \sum / \partial x_j$ is the cubical dilatation of the medium, ∇^2 is the Lagrangian operator, and Lamé's coefficients λ and μ refer to the elastic properties of the medium; λ controls the rate of growth or shrinkage of a local region whereas μ controls the shearing between adjacent regions of the image.

However, the assumption of linear elasticity restricts the registration to be globally smooth and therefore to accommodate only small deformations. In an extension to his initial work [5], Christensen [6] described an registration approach in which a viscous fluid model was used to control the deformation.

For viscous fluids, the force $\mathbf{F}(\mathbf{u})$ is proportional to the time rate of change in displacement. The PDE describing the fluid transformation of the template is given by (see, Christensen et al. [7] for a detailed derivation)

$$\nabla^2\mathbf{v} + (\lambda+\mu)\boldsymbol{\nabla}(\boldsymbol{\nabla}\cdot\mathbf{v}) = \mathbf{F}(\mathbf{u}), \tag{2}$$

where $\mathbf{v}$ is the instantaneous velocity of the displacement field $\mathbf{u}$. It is related to its displacement $\mathbf{u}$ by

$$\mathbf{v}(\mathbf{x},t) = \frac{\partial\mathbf{u}(\mathbf{x},t)}{\partial t} + \mathbf{v}(\mathbf{x},t)^T\boldsymbol{\nabla}\mathbf{u}(\mathbf{x},t). \tag{3}$$

The $\nabla^2\mathbf{v}$ term in (2) is the viscous term of the PDE. This term constraints the velocity of the neighboring particles of the displacement field to vary smoothly.

Due to attenuation in viscous fluids, internal forces disappear with time in this model. Thus, the desired deformation can be fully achieved, even if large deformations are required. Unfortunately, the original implementation is demanding with respect to its computational cost. Wollny and Kruggel [23] therefore proposed a fast algorithm to carry out non-rigid registration based on fluid dynamical modelling.

3 The Concept of Critical Points

Consider a vector field $\mathbf{u}\colon \Omega \to \mathbb{R}^3$ for some compact domain $\Omega \subseteq \mathbb{R}^3$ and the set:

$$U_\varepsilon(\mathbf{x}') := \{\mathbf{x} |\ \parallel \mathbf{x}-\mathbf{x}' \parallel < \varepsilon, \mathbf{x}\in\Omega\}, \tag{4}$$

for any $\varepsilon > 0, \varepsilon\in\mathbb{R}$ and a $\mathbf{x}'\in\Omega$; the set U_ε is called the *ε-environment* of $\mathbf{x}'$.

The Taylor series expansion of $\mathbf{u}(\mathbf{x})$ about the point $\mathbf{x}'$ yields:

$$\mathbf{u}(\mathbf{x}) = \left.\frac{\partial h_i}{\partial x_j}\right|_{\mathbf{x}'}(\mathbf{x}-\mathbf{x}') + \mathbf{u}(\mathbf{x}') + O(\mathbf{x}).$$

By taking into account only its linear terms, and with the substitution $\mathbf{A} := \left.\frac{\partial h_i}{\partial x_j}\right|_{\mathbf{x}'}, \mathbf{A}\in\mathbb{R}^{3\times3}$ we obtain

$$\mathbf{u}(\mathbf{x}) = \mathbf{A}(\mathbf{x}-\mathbf{x}') + \mathbf{u}(\mathbf{x}'). \tag{5}$$

Thus, we can now define [cf. 19]:

Definition 3.1. *A critical point $\mathbf{x}_{cp}$ is an equilibrium point in the vector field topology where $\mathbf{u}(\mathbf{x}_{cp}) = 0$ while there exists an $\varepsilon > 0, \varepsilon\in\mathbb{R}$ so, that $\mathbf{u}(\mathbf{x}) \neq 0\ \forall\,\mathbf{x}\in U_\epsilon(\mathbf{x}_{cp})\backslash\{\mathbf{x}_{cp}\}$.*

Proposition 3.1. *Within the vicinity of a critical point $\mathbf{x}_{cp}$, the vector field $\mathbf{u}(\mathbf{x})$–as it is outlined in* (5)*–can be approximated by*

$$\mathbf{u}(\mathbf{x}) = \mathbf{A}(\mathbf{x}-\mathbf{x}_{cp}),$$

where the matrix $\mathbf{A}$ is called the phase portrait *of the critical point $\mathbf{x}_{cp}$.*

As a first-order Taylor series would have a limited scope in modelling $\mathbf{u}(\mathbf{x})$ adequately, i.e., the influence of critical point $\mathbf{x}_{\text{cp}}$ would decay with distance $\Delta\mathbf{x} = \mathbf{x}-\mathbf{x}_{\text{cp}}$, accuracy in modelling can be increased by introducing the attenuation factor $1/\parallel \mathbf{x}-\mathbf{x}_{\text{cp}} \parallel^2$. Consequently, the approximation of $\mathbf{u}(\mathbf{x})$ now reads

$$\mathbf{u}(\mathbf{x}) = \frac{1}{\parallel \mathbf{x}-\mathbf{x}_{\text{cp}} \parallel^2}\mathbf{A}(\mathbf{x}-\mathbf{x}_{\text{cp}}). \tag{6}$$

A critical point may be classified with respect to the eigenvalues of $\mathbf{A}$ (as proposed by Abraham and Shaw [1]): we distinguish attractors, repellors, saddle points, and rotation centers (see Fig. 1).

For our intended application, namely to interpret morphological changes of the brain, attractors and repellors may describe areas of matter loss and growth, respectively, saddle points may characterize configurations at barriers or membranes, and rotation centers may indicate local tissue shearing.

4 Metric Space and Fix Points

In order to enhance the concept of critical points for our application, we will briefly review the concepts of metric spaces and contraction mapping (cf. also, Bronstein et al. [4] or Lu [15]). Here, we focus on attractors and repellors as other critical points are not necessarily represented by fix points. We discuss later, how saddle points and rotation centers may be detected.

4.1 Complete Metric Spaces

Given a set Θ, the function $d : \Theta \times \Theta \rightarrow [0, \infty)$ is called *metric* if, $\forall\, x, y, z \in \Theta$, all of the following three conditions hold:

$$\begin{aligned} &d(x,y) = 0 \Leftrightarrow x = y && \text{(identity)},\\ &d(x,y) = d(y,x) && \text{(symmetry)},\\ &d(x,y) \leq d(x,z) + d(y,z) && \text{(triangle inequality)}. \end{aligned}$$

Definition 4.1. *The pair (Θ, d) is called a* metric space.

Now, let $X = [x_i]_{i=0,1,\ldots}$ be a sequence in $\Theta \subseteq \tilde{\Theta}$, and $x \in \tilde{\Theta}$, then X is said to converge to x:

$$x_i \xrightarrow[i\rightarrow\infty]{} x \Leftrightarrow d(x_i, x) \xrightarrow[i\rightarrow\infty]{} 0. \tag{7}$$

X is said to be a *Cauchy sequence* in the metric space (Θ, d) if, $\forall\, \delta > 0, \delta \in \mathbb{R}$, there exists a $k \geq 0, k \in \mathbb{Z}$ such that $d(x_i, x_j) \leq \delta, \forall\, i, j \geq k$. This is equivalent to

$$d(x_i, x_j) \xrightarrow[i\rightarrow\infty]{} 0. \tag{8}$$

Definition 4.2. *A metric space (Θ, d) is said to be* complete *if any Cauchy sequence $X = [x_i]_{i=0,1,\ldots}$ converge to some point $x \in \Theta$.*

4.2 Contraction Mapping

Consider now a mapping $f : \Theta \rightarrow \Theta$ from one metric space onto itself. Such mapping is called a *transformation*, that is attributed as *contractive* on Θ if there exists a constant $s \in [0, 1)$ such that

$$d(f(x), f(y)) \leq s \cdot d(x, y) \qquad \forall\, x, y \in \Theta. \tag{9}$$

Any such constant s is called a *contractive factor* for the transformation f.

Theorem 4.1 (Contraction Mapping). *Let $f : \Theta \rightarrow \Theta$ be a contractive transformation on a complete metric space (Θ, d). Then f will possess exactly one point $a \in \Theta$ with $f(a) = a$; a is called* fix point *of a the transformation f. Moreover, the sequence $x, f(x), \ldots, f^k(x) := f(f^{k-1}(x)), \ldots$, or abbreviated*

$$\left[f^k(x)\right]_{k=0,1,\ldots}, \tag{10}$$

will converge for any $x \in \Theta$ to the fix point a, i.e.

$$\lim_{k\rightarrow\infty} f^k(x) = a. \tag{11}$$

Proof. Consider two fix points $a, \tilde{a} \in \Theta$. According to (9)

$$d(f(a), f(\tilde{a})) \leq s \cdot d(a, \tilde{a})$$

hold, and, as a and $\tilde{a}$ are fix points,

$$d(a, \tilde{a}) \leq s \cdot d(a, \tilde{a}).$$

With $s \in [0, 1)$ we conclude that $d(a, \tilde{a}) = 0$ and $a = \tilde{a}$.

Accounting now for the sequence (10) and the fix point a we yield accordingly:

$$d(f^k(x), f(a)) = d(f^k(x), a) \leq s^k \cdot d(x, a).$$

With $s \in [0, 1)$ follows:

$$s^k \xrightarrow[k\rightarrow\infty]{} 0,$$

thus

$$d(f^k(x), a) \xrightarrow[k\rightarrow\infty]{} 0,$$

and with (7)

$$\lim_{k\rightarrow\infty} f^k(x) = a.$$

□

A fix point such as a is called *attraction point* within Θ.

4.3 Attractors and Repellors as Fix Points of Contractive Transformations

Reconsider the vector field $\mathbf{u} \colon \Omega \rightarrow \mathbb{R}^3$ from section 3 that is defined on some compact domain $\Omega \subseteq \mathbb{R}^3$. A transformation $\mathbf{T} \colon \Omega \rightarrow \Omega$, as it is achieved by non-rigid image registration (cf. section 2) may be assumed, so that

$$\mathbf{T}(\mathbf{x}) = \mathbf{x} + \mathbf{u}(\mathbf{x}). \tag{12}$$

Here, each image is defined to be a function of $\mathbf{x} \in \Omega = [0, 1]^3$, and $\mathbf{T}$ is a vector-valued function of $\mathbf{x} \in \Omega \rightarrow \Omega$ that resides in an Euclidean reference frame. The metric space is defined by the pair (Ω, d), where d is the Euclidean distance:

$$d(\mathbf{x}, \mathbf{y}) := \| \mathbf{x} - \mathbf{y} \|_2, \qquad \forall\, \mathbf{x}, \mathbf{y} \in \Omega.$$

As Ω is compact, any Cauchy sequence $X = [\mathbf{x}_k]_{k=0,1,\ldots}$ converges to

$$\lim_{k\rightarrow\infty} \mathbf{x}_k = \mathbf{x} \in \Omega,$$

thus, the pair (Ω, d) is a complete metric space. We may hence consider fix points of $\mathbf{T}$ according to section 4.2.

Definition 4.3. *For a fix point* $\mathbf{a} \in \Omega$*, the set*

$$\Theta(\mathbf{a}) := \left\{ \mathbf{x} | \mathbf{x} \in \Omega \wedge \lim_{k \to \infty} \mathbf{T}^k(\mathbf{x}) = \mathbf{a} \right\} \qquad (13)$$

is called contraction area *Θ of* $\mathbf{a}$*.*

For the following discussion of the phase portrait of $\mathbf{a}$ we will now, exemplarily, only account for fix points if a constant $\delta > 0, \delta \in \mathbb{R}$ exists with

$$\tilde{\Theta} := \{\mathbf{x} | \parallel \mathbf{x} - \mathbf{a} \parallel_2 < \delta \wedge \delta > 0\} \subseteq \Theta(a), \qquad (14)$$

i.e., the attraction area of fix point $\mathbf{a}$ consists of at least a sphere with radius δ around $\mathbf{a}$.

According to (6), we obtain

$$\mathbf{A}(\mathbf{x} - \mathbf{a}) \approx \parallel \mathbf{x} - \mathbf{a} \parallel_2 \mathbf{u}(\mathbf{x}).$$

Finally, as $\mathbf{a} \rightarrow \mathbf{x} + \mathbf{u}(\mathbf{x})$ for $\mathbf{x} \rightarrow \mathbf{a}$, and substituting $\lambda = \parallel \mathbf{x} - \mathbf{a} \parallel_2$ we have

$$\mathbf{A}\mathbf{u}(\mathbf{x}) \approx -\lambda \mathbf{u}(\mathbf{x}).$$

This result accounts for all vectors $\mathbf{u}(\mathbf{x}) \in \tilde{\Theta}$. According to (14), the set $\tilde{\Theta}$ may also contain the eigenvectors of $\mathbf{A}$. Then, all its three eigenvalues must be less than zero ($\lambda_1 \leq \lambda_2 \leq \lambda_3 < 0$), and the fix point $\mathbf{a}$ is called *attractor* (see Fig. 1).

If re-formulating the transformation function $\mathbf{T}$ in (12) by

$$\mathbf{T}_{\text{inv}}(\mathbf{x}) = \mathbf{x} - \mathbf{u}(\mathbf{x}), \qquad (15)$$

the fix point of sequence $\left[\mathbf{T}^k_{\text{inv}}(\mathbf{x})\right]_{k=0,1,\ldots}$ correspond to repellor. The respective derivation is analogous to the one above.

4.4 Estimation of Critical Points

When registering morphological changes we obtain vector fields—the displacements—that are not given on a continuous domain Ω, but on its discretization $\hat{\Omega}$ which reflects the finite resolution of the images. As discussed in the introduction, a critical point in our application domain is not infinitesimally small, but merely represents a zone where the vector field is attracted to or repelled from, for example.

By its mathematical foundation, our method is able to detect attractors or repellors, only. If a saddle point is unbalanced, i.e. the inflow of matter is not equal to the outflow, or if a rotation center attracts/repells during the morphological change that is registered, then we are able to detect them by contraction mapping.

As we are seeking for an approximation of vector field $\mathbf{u}(\mathbf{x})$ in the environment of a critical point $\mathbf{x}_{\text{cp}}$, we substitute $\Delta\mathbf{x} := \mathbf{x} - \mathbf{x}_{\text{cp}}$ in (6) and yield:

$$\parallel \Delta\mathbf{x} \parallel \mathbf{u}(\mathbf{x}_{\text{cp}} + \Delta\mathbf{x}) = \mathbf{A}(\Delta\mathbf{x}). \qquad (16)$$

Accounting for a certain environment around $\mathbf{x}_{\text{cp}}$, with (16) we obtain an over-determined system of linear equations

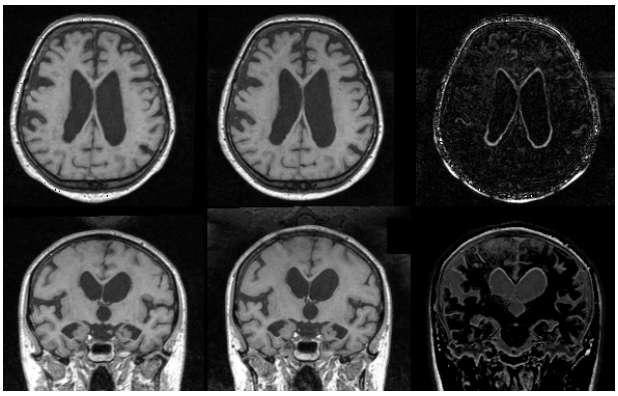

Fig. 2. Axial slice 90 (top row) and coronal slice 140 (bottom row) from $200 \times 256 \times 200$ voxel MR data sets taken 3 months (left panel) and 15 month (middle panel) after the patients' accident. The right panel shows the difference between both images.

[19] which can be solved by using Householder transformations [21]. As the phase portrait A is 3×3 matrix, its eigenvalues can be calculated easily by solving the characteristic equation

$$\det(\mathbf{A} - \lambda \mathbf{I}) = 0$$

using Cardan's formula [4]. Critical points are classified by examining their eigenvalues (see Fig. 1).

5 Application—Visualization of shape change

We applied our algorithm to magnetic resonance (MR) images of a patient suffering from a bi-frontal severe head contusion (trauma) as a consequence of a car accident. According to the current model of trauma pathogenesis, free oscillations dispersed within the brain after the impact, leading to shear stresses and (micro) hemorrhages, and consequently, to a local destruction of brain tissue, which is removed during recovery. The resulting matter loss should be compensated by an increase in cerebro spinal fluid (CSF). Analyzing the pattern of matter loss is important to improve the understanding of the pathological process induced by the trauma.

The patient was scanned 3 months and 15 months after the trauma (Fig. 2). Both datasets were registered by the fluid dynamic, non-rigid approach described in section 2. We obtained a displacement vector at every point of the reference image, corresponding to the shift of tissue during the time interval. Fig. 3 serves as a first example to visualize such morphological change. The ventricular system (the low-intense cavities within the brain in Fig. 2) was segmented from the brain. The spatial pattern of shape change is visualized as follows: for each point on the ventricular surface, the displacement vector is decomposed into its normal and tangential components. Inward-pointing normals are coded in red, outward-pointing in blue; colour intensity reflects its magnitude. The scale is given in mm. The displacement vectors are shown as arrows. It is interesting to note that the ventricles are clearly enlarged, most notable in superior direction. This a consequence of a loss of brain tissue, resulting in an increase

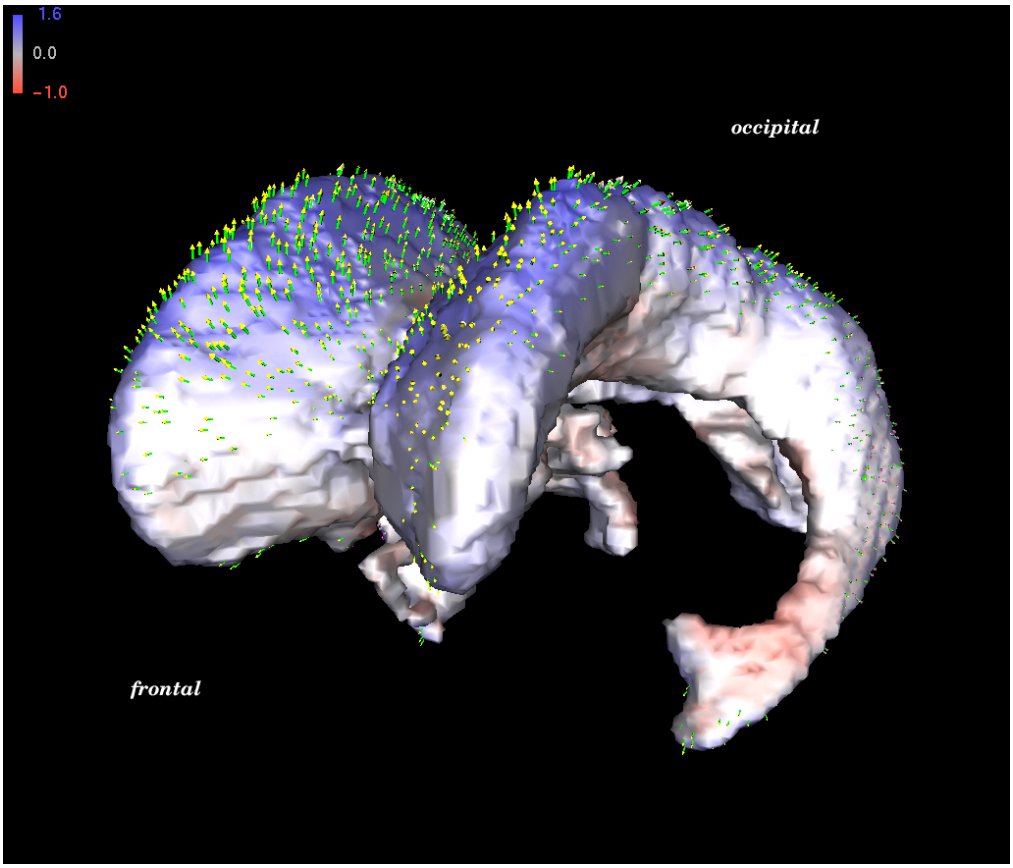

Fig. 3. Shape difference of a patients' ventricular system between two examination time points (see text). The colour indicate the orientation and magnitude of shape difference; arrows indicate the displacements. Note the overall enlargement of the system which is a consequence of the tissue loss (atrophy) of the surrounding brain.

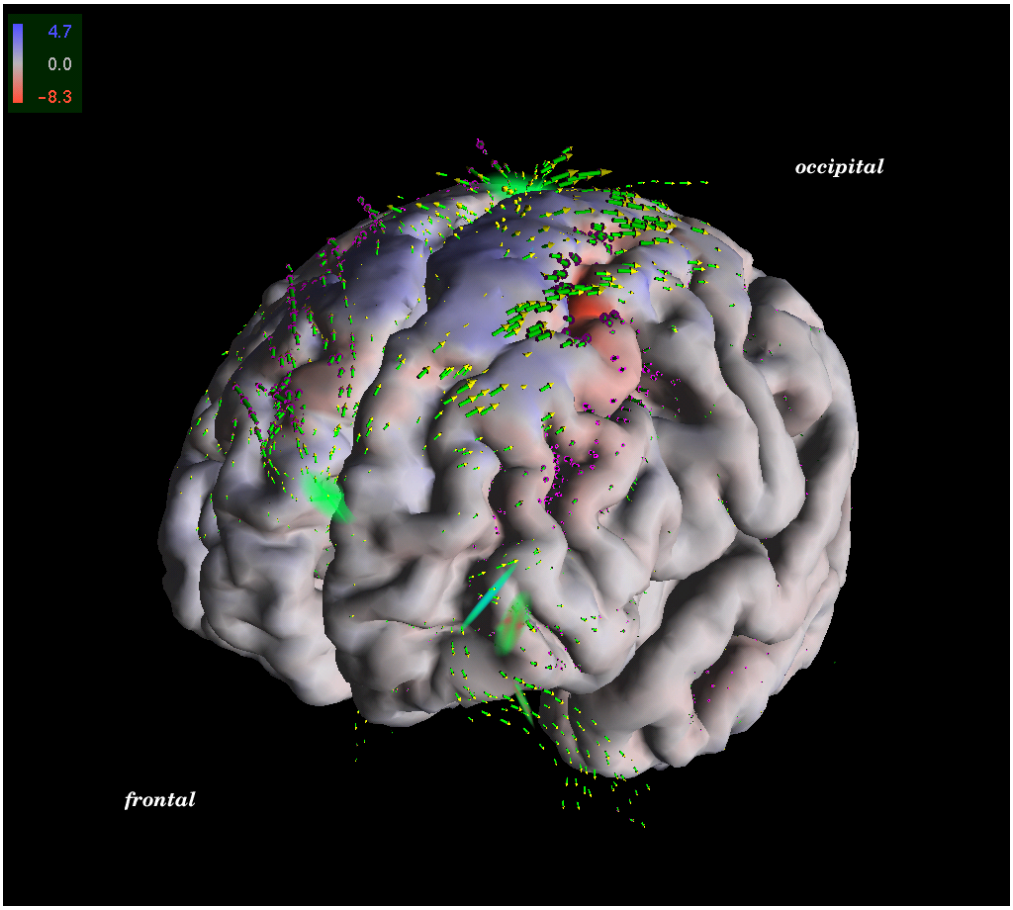

Fig. 4. Pattern of shape change of a patients' brain between two examination time points. Changes in morphology are visualized by colours; red and blue indicate inward and outward direction, respectively, and the magnitude of shape change perpendicular to the surface of the brain. The major displacement lines (arrows) depict the deformation lines. The critical point (repellor) within the frontal CSF compartment indicates a virtual flow in fronto-occipital direction.

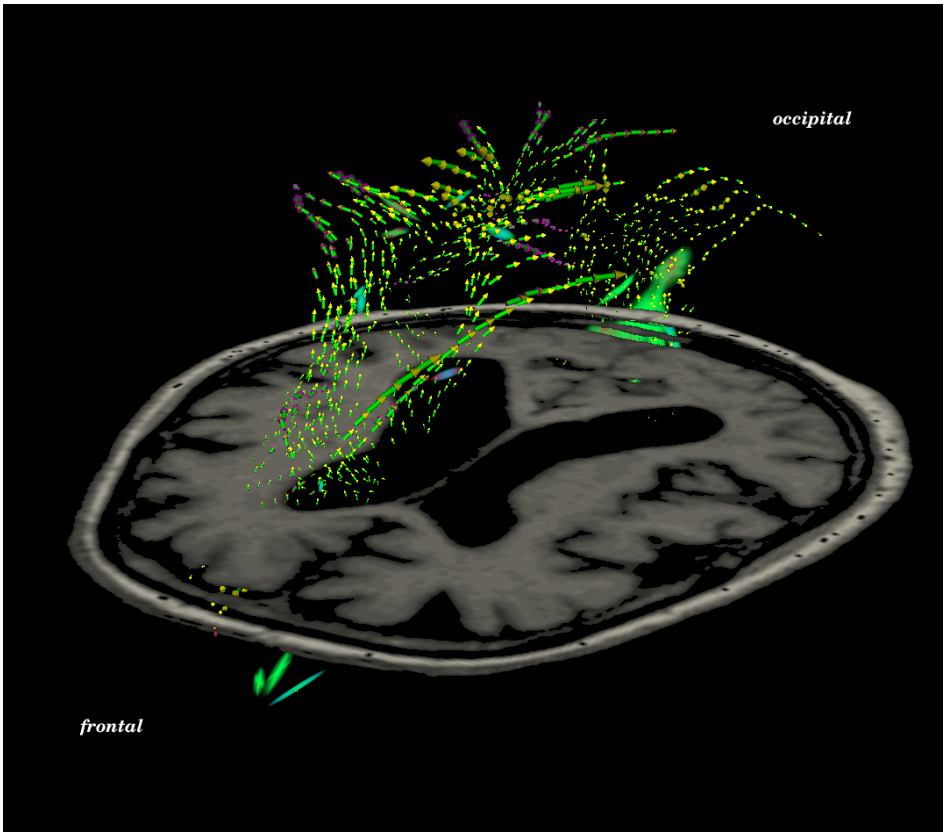

Fig. 5. View of an axial slice (taken from Fig. 4) with major displacement lines and critical points of high magnitude. A repellor (green object) in the frontal cerebro-spinal fluid (CSF) and the displacement lines depict a virtual flow in occipital direction. Saddle points of type II (cf. Fig. 1) with strong repelling properties (green part) lie within the occipital CSF; those reveal a retraction of the brain. Small attractors (red) some with rotation properties (red-magenta) presumably correspond to areas a regionally more profound matter loss.

in the CSF volume. The superior orientation of the ventricular enlargement indicate a more profound tissue damage in the supra-ventricular compartment.

From the displacement field we extracted critical points. To represent their properties, a colour scheme is implemented, where green and red indicate repelling or attracting property, and blue a rotation component. With this colour-code a critical point could be easily visualized: a repellor appears purely green, an attractor red, and a rotation center blue. Different types of saddle points may be distinguished by mixing the respective colours.

The set of critical points is dominated by a strong repellor locate in the pre-frontal CSF compartment (Fig. 4), and by several saddle points with strong repelling properties within the occipital CSF compartment (Fig. 5). Since the trauma occurred on the forehead, a focus of matter loss is in the frontal lobes, leading to an increase of the CSF component close to the frontal pole. Displacement stream lines (Figs. 4 and 5) map the ”flow” of tissue along the mid line structures (as a correlate of a global atrophy) and reveal a retraction of the brain in the frontal-occipital direction. The occipital saddle point (Fig. 5) can be interpreted as a backward shift of the brain, while pushing CSF in the repelling direction. As could be deduced by Fig. 4 the strongest deformations occur in the posterior portions of the first and second frontal gyrus on both hemispheres.

6 Conclusion

We proposed to describe displacement fields obtained from non-rigid registration of temporal series of MR images by its critical points. We introduced a novel method for finding critical points in discrete vector fields, is based on contraction mapping.

However, our method fails to detect some specific critical points, such as rotation centers or balanced saddle points. Here, local measures based on the Jacobian [14] or global approaches like recently introduced by Polthier and Preuß [20] will be integrated with this method.

The advantage of conducting a biomedical analysis over simple visual comparison as carried out in clinical routine is obvious: the consequences of the bifrontal head trauma are understood as a circumscribed tissue loss leading to quantifiable deformations of the brain structures.

Acknowledgements. Research of M.T. and G.W. is supported by the IST V programme of the European Union (SimBio project, No. 10378).

References

1. R. H. Abraham and C. D. Shaw. *Dynamics–The Theory of Behavior*. Addison-Wesley, Redwood (Ca), 2nd edition, 1992.
2. Y. Amit. A nonlinear variational problem for image matching. *Soc. Ind. Math.*, 15(1):207–224, 1994.
3. F. L. Bookstein. Landmark methods for forms without landmarks: morphometrics of group differences in outline shape. *Med. Image Anal.*, 1(3):225–243, 1997.
4. I. N. Bronstein, K. A. Semendjajev, G. Musiol, and H. Mühlig. *Taschenbuch der Mathematik (in german)*.

Verlag Harry Deutsch, Thun · Frankfurt/M., 5th edition, 2001.
5. G. E. Chistensen, R. D. Rabbit, and M. I. Miller. 3D brain mapping using deformable neuroanatomy. *Phys. Med. Biol.*, 39:609–618, 1994.
6. G. E. Christensen. *Deformable shape models for neuroanatomy*. DSc.-thesis, Server Institue of Technology, Washington University, Saint Louis, 1994.
7. G. E. Christensen, R. D. Rabbitt, and M. I. Miller. Deformable templates using large deformation kinematics. *IEEE Trans. Medical Imag.*, 5(10):1435–1447, Oct. 1996.
8. Johnson H. J. Christensen, G. E. Consistent image registration. 20(7):568–582, 2001. IEEE Trans. Medical Imag.
9. J. C. Gee, M. Reivich, and R. Bajcsy. Elastically deforming atlas to match anatomical brain images. *J. Comp. Assisted Tomography*, 17:255–236, 1993.
10. D. H. Gottlieb and G. Samaranayake. The index of discontinuous vector fields. *New York J. Math.*, 1:130–148, 1995.
11. U. Grenander and M. I. Miller. Computational anatomy: An emerging discipline. *Quaterly Appl. Math.*, LVI(4): 617–694, Dec. 1998.
12. H.-C. Hege and K. Polthier, editors. *Mathematical visualization : algorithms, applications and numerics*. Springer, Berlin, 1998.
13. J. L. Helman and L. Hesselink. Representation and display of vector field topology in fluid flow data sets. *IEEE Computer*, 22(8):27–36, August 1989.
14. J. L. Helman and L. Hesselink. Visualizing vector field topology in fluid flows. *IEEE Computer Graphics & Applications*, 11(3):36–46, May 1991.
15. N. Lu. *Fractal Imaging*. Academic Press, San Diego, CA, 1997.
16. J. B. A. Maintz and M. A. Viergever. A survey of medical image registration. *Medical Image Analysis*, 2(1):1–36, 1998.
17. M. I. Miller, G. E. Christensen, Y. Amit, and U. Grenander. Mathematical textbook of deformable neuroanatomies. In *Proc. Natl. Acad. Sci. USA 90*, pages 11.944–11.948, 1993.
18. O. Musse, F. Heintz, and J.-P. Armspach. Topology preserving deformable image matching using constraint hierachical parametric models. *IEEE Trans. Medical Imag.*, 10(7):1081–1093, July 2001.
19. P. A. Philippou and R. N. Strickland. Vector Field Analysis and Synthesis Using Three-Dimensional Phase Portraits. *Graphical Models And Image Processing*, 6(59): 446–462, 1997.
20. K. Polthier and E. Preuß. Detecting vector field singularities from potentials. http://www-sfb288.math.tu-berlin.de/ konrad/articles.html, 2001.
21. W. H. Press, S. A. Teukolsky, W. T. Vetterling, and B. P. Flannery. *Numerical Recipes in C. The Art of Scientific Computing*. Cambridge Univ. Press, New York, 2nd edition, 1992.
22. G. Scheuermann, H. Hagen, and H. Krüger. Clifford algebra in vector field visualization. In H.-C. Hege and K. Polthier, editors, *Mathematical Visualization*, pages 343–351. Springer-Verlag, Heidelberg, 1998.
23. G. Wollny and F. Kruggel. Computational cost of nonrigid registration algorithms based on fluid dynamics. submitted to IEEE Trans. Medical Imag., 2000.